Atmos. Chem. Phys. Discuss., https://doi.org/10.5194/acp-2018-482
Manuscript under review for journal Atmos. Chem. Phys.
Discussion started: 29 May 2018

Atmospheric Chemistry and Physics Discussions

A new interpretative framework for below-cloud effects on stable water isotopes in vapour and rain

Pascal Graf[1], Heini Wernli[1], and Harald Sodemann[1,2,3]

[1]Institute for Atmospheric and Climate Science, ETH Zurich, Zurich, Switzerland
[2]Geophysical Institute, University of Bergen, Bergen, Norway
[3]Bjerknes Centre for Climate Research, Bergen, Norway

Correspondence: Pascal Graf (pascal.graf@env.ethz.ch)

Abstract. Raindrops interact with water vapour in ambient air while sedimenting from the cloud base to the ground. They constantly exchange water molecules with the environment and, in sub-saturated air, they evaporate partially or entirely. The latter of these below-cloud processes is important for predicting the resulting surface rainfall amount and it influences the boundary layer profiles of temperature and moisture through to evaporative latent cooling and humidity changes. However, despite its importance, it is very difficult to quantify this process from observations. Stable water isotopes provide such information, as they are influenced by both rain evaporation and equilibration. This study elucidates this option by introducing a novel interpretation framework for stable water isotope measurements performed simultaneously at high temporal resolution in both near-surface vapour and rain. We refer to this viewing device as the $\Delta\delta\Delta d$-diagram, which shows the isotopic composition (δ^2H, d-excess) of equilibrium vapour from precipitation samples relative to the ambient vapour. It is shown that this diagram facilitates the diagnosis of below-cloud processes and their effects on the isotopic composition of vapour and rain since equilibration and evaporation lead to different pathways in the two-dimensional phase space of the $\Delta\delta\Delta d$-diagram. For a specific cold front in Central Europe, the analysis shows that below-cloud processes lead to distinct and temporally variable imprints on the isotope signal in surface rain. The influence of evaporation on this signal is particularly strong during periods with a weak precipitation rate. After the frontal passage, the near-surface atmospheric layer is characterised by higher relative humidity and a lower melting layer, leading to weaker below-cloud evaporation and equilibration. Measurements from four cold frontal events reveal a surprisingly similar slope of $\frac{\Delta d}{\Delta \delta} = -0.30$ in the phase space, indicating a potentially characteristic signature of below-cloud processes for this type of rain events.

1 Introduction

Processes acting during the short travel of rain through the atmosphere from cloud base to the surface has a, maybe surprisingly, large relevance for several atmospheric phenomena. The two-phase system of rain and vapour is in constant molecular exchange. In addition, in unsaturated conditions, rain partially evaporates, leading to latent cooling of the air, and moistening of the boundary layer. Surface rainfall totals may be substantially lower in cases of strong evaporation (Aemisegger et al., 2015), and in the case of convection in the Sahel, large evaporation-driven cold pools can trigger extensive dust storms known

Atmos. Chem. Phys. Discuss., https://doi.org/10.5194/acp-2018-482
Manuscript under review for journal Atmos. Chem. Phys.
Discussion started: 29 May 2018

Atmospheric Chemistry and Physics Discussions

as haboobs (Roberts and Knippertz, 2012). In mid-latitudes, cold pool formation influences low-level moisture convergence and thereby the progression and organisation of convective systems (Bennett et al., 2007).

Measurements of these so-called below-cloud processes (Aemisegger et al., 2015) are challenging. Common radiosondes provide instantaneous snapshots of a vertical profile of humidity and temperature, but do not capture precipitation rates, and are expensive when deployed at high frequency. Radar data on the other hand can continuously provide vertically resolved drop spectra, but do neither provide relative humidity nor temperature, which are necessary to reasonably quantify precipitation evaporation (Xie et al., 2016). Other remote-sensing systems, such as Raman water vapour lidar (Cooney, 1970), Fourier transform infrared radiometers (Schneider and Hase, 2009) and passive microwave radiometers (Solheim et al., 1998) provide vertical profiles of humidity, but are strongly attenuated during precipitation.

As a consequence of the lack of sufficient observations, models use poorly constrained parameters to represent the interaction of falling raindrops with the air column below the cloud base. Errors in the representation of this process diminishes the model forecast quality due to its impact on the rainfall amount and the dynamics of a weather system. This issue becomes even more relevant as weather prediction models progress to resolution beyond the grey zone, where precipitation is a prognostic variable (COSMO, AROME, WRF; Steppeler et al., 2003; Seity et al., 2010; Skamarock et al., 2008), and convective updrafts, downdrafts and the formation of cold pools are partly resolved at the grid scale. These modelling challenges provide an additional motivation to deepen our understanding of below-cloud processes.

In this context, stable isotopes of water vapour and rain are useful to investigate below-cloud processes. Stable water isotopes are natural, passive tracers that integrate over the phase-change history of water. The stable isotope composition is quantified using isotope ratios, defined as the concentration of the rare (heavy $^{2}\mathrm{H}^{1}\mathrm{H}^{16}\mathrm{O}$ or $^{1}\mathrm{H}_{2}^{18}\mathrm{O}$) over the abundant (light $^{1}\mathrm{H}_{2}^{16}\mathrm{O}$) isotope, e.g.:

$$^{2}R = \frac{[^{2}\mathrm{H}^{1}\mathrm{H}^{16}\mathrm{O}]}{[^{1}\mathrm{H}_{2}^{16}\mathrm{O}]} \tag{1}$$

Most studies use the more intuitive δ notation (Dansgaard, 1964; Galewsky et al., 2016), which expresses the heavy isotope composition of a reservoir in terms of relative deviation of R from an internationally accepted standard:

$$\delta = \frac{R_{\mathrm{sample}} - R_{\mathrm{standard}}}{R_{\mathrm{standard}}} \tag{2}$$

A δ value is defined for both heavy over light isotope concentrations ($\delta^{2}\mathrm{H}$ and $\delta^{18}\mathrm{O}$) and generally indicated in per mil (‰) relative to Vienna Standard Mean Ocean Water (VSMOW2; IAEA, 2009). As heavy isotopes preferentially condense due to their larger mass, vapour in higher levels of the atmosphere are increasingly depleted of heavy isotopes, reflected in negative δ values. As precipitation forms from this vapour depleted in heavy isotopes, temperature-dependent fractionation will lead to a relative enrichment of heavy isotopes in the precipitation. Typically, though, precipitation δ values will still be depleted relative to the standard ocean water VSMOV2, as expressed in negative delta values. As precipitation falls through the air column, the drop and the surrounding vapour will continuously exchange water molecules. Thermodynamics will direct this exchange towards isotopic equilibrium according to ambient temperature. This process is termed *equilibration* and only occurs when the precipitation is liquid.

Atmos. Chem. Phys. Discuss., https://doi.org/10.5194/acp-2018-482
Manuscript under review for journal Atmos. Chem. Phys.
Discussion started: 29 May 2018

Atmospheric Chemistry and Physics Discussions

In unsaturated conditions, a net transfer of water molecules from the drops to the surrounding air does occur. The second-order parameter d-excess ($d = \delta^2\mathrm{H} - 8 \cdot \delta^{18}\mathrm{O}$) is sensitive to such non-equilibrium conditions, where $^2\mathrm{H}^1\mathrm{H}^{16}\mathrm{O}$ reaches isotopic equilibrium faster than $^1\mathrm{H}_2^{18}\mathrm{O}$. The d-excess quantifies the difference in $^2\mathrm{H}^1\mathrm{H}^{16}\mathrm{O}$ and $^1\mathrm{H}_2^{18}\mathrm{O}$ from their ratio expected during equilibrium conditions as a measure of non-equilibrium (Dansgaard, 1964; Stewart, 1975). Further parameters critically influence this process, such as the drop size distribution (Managave et al., 2016), below-cloud relative humidity (Lee and Fung, 2008), the height of the melting layer, the height of the cloud base (Wang et al., 2016), and vertical wind velocity. Thus, isotopes reflect the conditions acting on rain below the cloud, but in convoluted ways that often render interpretation cumbersome.

Previous studies often investigated only one part of the two-phase system (e.g., Miyake et al., 1968; Celle-Jeanton et al., 2004; Barras and Simmonds, 2009; Risi et al., 2010; Muller et al., 2015; Managave et al., 2016). They studied rain in high temporal resolution and came up with partially contrasting explanations for the observed short-term isotopic variations. For example, Coplen et al. (2008) and Yoshimura et al. (2010) investigated an atmospheric river event in California and disagreed on whether below-cloud processes or changes in the formation height caused the variations they observed. Aemisegger et al. (2015) showed for a mid-latitude rain event that joint observations in vapour and rain reveal the influence of below-cloud processes more clearly and contain information on the structure of the precipitation system.

Since vapour and rain are in a continuous exchange, measuring one without the other makes meaningful interpretation difficult. This is especially the case in situations dominated by advection, for example cold-frontal rain. There, the isotopic evolution of rain is a combined signal of a changing air mass and cloud signal, below-cloud equilibration with progressively depleted vapour as the front progresses, and rain evaporation (Dütsch et al., 2016). Simultaneous observations of vapour and precipitation are necessary to distinguish these processes and quantify below-cloud processes.

Thus, joint observations of the stable isotope composition of vapour and precipitation at ground level are valuable, as they contain the convoluted influence of different factors and processes. However, for the same reason, extracting the main driving factors is a difficult task. Here we introduce a new set of measures to single out the influences of equilibration and evaporation on the isotope composition of near-surface vapour and rainfall. Using high-resolution joint isotope data from cold fronts in Central Europe, we introduce a new viewing and interpretation device, which allows to determine the leading below-cloud processes during a precipitation event.

2 Data and Methods

2.1 Isotope measurements

Stable water isotopes in ambient water vapour were measured on a tower building at the Institute for Atmospheric and Climate Science of ETH Zurich (47.38°N, 8.55°E; 510 m a.s.l) between 9 October and 27 November 2015 with a cavity ring down spectrometer (L1115-i, Picarro Inc, USA). Ambient air was directed to the analyser through a 10 m PFA tubing heated to 70°C that was flushed by a bypass pump (HN022AN.18, KNF Neuberger, Germany) with a flow rate of 9 $l\,\mathrm{min}^{-1}$ (Aemisegger et al., 2012; Aemisegger, 2013). The isotopic analyser was calibrated twice a day at ambient humidity levels using a commercial setup (Standards Delivery Module A0101 and Vaporizer V1102-i, Picarro Inc. USA). Two laboratory standards bracketing the com-

Atmos. Chem. Phys. Discuss., https://doi.org/10.5194/acp-2018-482
Manuscript under review for journal Atmos. Chem. Phys.
Discussion started: 29 May 2018

Atmospheric Chemistry and Physics Discussions

position of typical ambient values in ambient vapour (Standard 1: $\delta^2\mathrm{H} = -75‰$, $\delta^{18}\mathrm{O} = -10‰$; Standard 2: $\delta^2\mathrm{H} = -247‰$, $\delta^{18}\mathrm{O} = -43‰$) were provided to the analyser for 15 min each. Raw measurements were corrected with an average calibration function from all calibration runs of the measurement period. Frequent gaps in the calibration make this time-independent calibration function more robust compared to the usual linear interpolation between subsequent calibration runs. The thereby neglected shorter-term drift leads to an increased uncertainty of the calibrated measurements. The 5 s measurements of the instrument were transformed to 10 min average values, which have an average uncertainty after calibration of 1.23‰ for $\delta^2\mathrm{H}$, 0.42‰ for $\delta^{18}\mathrm{O}$, and 3.6‰ for d-excess. For more details about the vapour isotope measurements, see Graf (2018).

At the same location, rain was manually sampled during selected events with a simple rainfall collector. The collector consists of a PTFE funnel of 15 cm diameter, which points into a 20 ml glass vial. Each sample was collected in a separate vial, which was immediately closed after retrieval from the sampler to avoid evaporation after sampling. A default sampling interval of 10 min was applied, which was shortened to 5 min during intense rain, or prolonged up to 30 minutes if the sampled amount was not sufficient for analysis. The approximate sample amount was recorded, but not used to determine rain rates. The samples were analysed for their isotopic composition in the laboratory with a cavity ring down spectrometer (L2130-i, Picarro Inc., USA) operating for liquid sample analysis (Graf, 2018). The average uncertainty of the calibrated liquid samples is 1.25‰ for $\delta^2\mathrm{H}$, 0.24‰ for $\delta^{18}\mathrm{O}$ and 1.43‰ for d-excess. In this study, 86 continuous rainfall samples collected during a cold frontal passage on 20 November 2015 are presented.

Also measured at the same location were temperature, humidity, wind speed and direction, and precipitation amount and intensity. These parameters were obtained at a 10 min interval from different meteorological sensors (Thygan VTP37 and wind gauge WN37, meteolabor AG; Tipping bucket rain gauge 7051.1000, Theodor Friedrichs & Co.) on the rooftop with measurement distance of less than 5 m to the ambient air inlet of the isotopic analyser.

2.2 Equilibrium vapour from precipitation

Rain falling from the clouds and the vapour in the atmospheric column below compose a two-phase system. The liquid precipitation and the surrounding water vapour exchange water molecules during fall, leading towards an equilibrium in the isotopic composition of both phases. In equilibrium, there is no net exchange of molecules between the phases, i.e., the exchange in both directions is equal for all isotopic species. Temperature-dependent isotopic fractionation between light and heavy isotopes however gives rise to different isotopic compositions of the liquid and vapour phases in equilibrium:

$$R_l = \alpha_{v\to l}\, R_v\,, \tag{3}$$

which can be equivalently expressed in δ-notation as

$$\frac{\delta_l}{1000} + 1 = \alpha_{v\to l}\left(\frac{\delta_v}{1000} + 1\right). \tag{4}$$

Here, subscripts l and v denote the liquid and vapour phase, respectively, and $\alpha_{v\to l}$ is the temperature-dependent fractionation factor of the vapour to liquid phase transition. At 20°C, $\alpha_{v\to l}$ is 1.0850 for ${}^2\mathrm{H}^1\mathrm{H}^{16}\mathrm{O}/{}^1\mathrm{H}_2^{16}\mathrm{O}$ and 1.0098 for ${}^1\mathrm{H}_2^{18}\mathrm{O}/{}^1\mathrm{H}_2^{16}\mathrm{O}$ (Majoube, 1971).

Atmos. Chem. Phys. Discuss., https://doi.org/10.5194/acp-2018-482
Manuscript under review for journal Atmos. Chem. Phys.
Discussion started: 29 May 2018

Atmospheric Chemistry and Physics Discussions

We denote the difference between the two phases due to fractionation in equilibrium as *equilibrium difference* Δ_{l-v}. The equilibrium difference makes it cumbersome to judge whether two phases are in equilibrium from comparing their δ-values only. The dependence of the equilibrium difference on temperature and isotopic composition further complicates matters, in particular for the interpretation of the d-excess (Dütsch et al., 2016).

Consider, for example, the equilibrium difference for a vapour-liquid system, where the liquid has a composition of 0‰ for both δ^2H and δ^{18}O (A in Table 1). Δ_{l-v} for δ^2H at 20°C is 78.4‰ and 101.0‰ at 0°C. Thus, equilibrium fractionation for cold temperatures is stronger and leads to a larger equilibrium difference of δ^2H and δ^{18}O. In addition, these differences are smaller if the liquid is more depleted in heavy isotopes. For a liquid with $\delta^2\mathrm{H} = -120‰$, Δ_{l-v} becomes 69.0‰ at 20°C, and 88.9‰ at 0°C (B in Table 1). The increase in fractionation strength with decreasing temperature is stronger for δ^2H than for δ^{18}O, which leads to a more positive equilibrium difference for d towards colder temperatures. In addition, d of vapour increases and hence the equilibrium difference decreases if the liquid or solid is depleted in heavy isotopes.

The problem that the comparison of δ-values in precipitation and ambient vapour is not straightforward can be overcome by comparing the isotopic composition of ambient vapour with the *equilibrium vapour from precipitation* for δ-values and d, termed $\delta_{\mathrm{p,eq}}$ and $d_{\mathrm{p,eq}}$ (Aemisegger et al., 2015). The equilibrium vapour from precipitation is defined as the calculated composition of a vapour that is in exact equilibrium with precipitation, where ambient air temperature is used in the calculation. The direction of isotopic exchange then becomes apparent directly from the difference between $\delta_{\mathrm{p,eq}}$ and δ_{v} for the δ-values, and from comparing $d_{\mathrm{p,eq}}$ and d_{v} for the d-excess. This substantially simplifies the interpretation of the state of equilibrium in the liquid-vapour system.

Therefore, in the following we make use of the isotopic composition of the *equilibrium vapour from precipitation*. Differences between ambient vapour and precipitation are thereby denoted as:

$$\Delta\delta = \delta^2\mathrm{H}_{\mathrm{p,eq}} - \delta^2\mathrm{H}_{\mathrm{v}} \quad \text{and} \tag{5}$$

$$\Delta d = d_{\mathrm{p,eq}} - d_{\mathrm{v}}. \tag{6}$$

A $\Delta\delta$ could also be defined for δ^{18}O, which would require an additional index for $\Delta\delta$ to discriminate between δ^2H and δ^{18}O. Since information about δ^{18}O is already included in d, only δ^2H will be used in this study and the notation is confined to $\Delta\delta$.

In the analysis below, we will use $\Delta\delta$ and Δd as introduced here as measures of the deviation of the vapour-precipitation system from equilibrium. It will be shown that this results in a powerful, intuitive interpretative framework to quantify physical processes between cloud base and surface from highly-resolved stable isotope measurements in water vapour and precipitation.

3 Cold frontal passage on 20 November 2015

We will apply the framework outlined above to data from a prolonged rainfall period in northern Switzerland. High-resolution rain and vapour isotope measurements reveal variations in the below-cloud processes during the event.

Atmos. Chem. Phys. Discuss., https://doi.org/10.5194/acp-2018-482
Manuscript under review for journal Atmos. Chem. Phys.
Discussion started: 29 May 2018

Atmospheric Chemistry and Physics Discussions

3.1 Meteorological situation

The local meteorology of this event was characterised by an extended front over Central Europe, which was the remnant of a cold front associated with a decaying cyclone over the Gulf of Finland. The nearly zonally oriented front passed Switzerland from a northerly direction during 20 November 2015, before leading to the genesis of a new cyclone over the Gulf of Genoa on the following day. The rainband associated with the cold front extends zonally over a distance of about 400 km from the Burgundy (France) across Switzerland to the Lake Constance, with a distinct band of high rain intensity (Fig. 1a). This intense rainband was embedded in a broader zone with stratiform rain. Near Zurich, the frontal passage led to a decrease of equivalent potential temperature (Θ_e) at 850 hPa of more than 12 K and to a veering of the wind from southwest to northwest (Fig. 1b).

3.2 Meteorological surface observations

An overview of selected surface measurements between 06 UTC 20 November and 01 UTC 21 November 2015 is shown in Fig. 2. The local 2-m temperature (T; red line in Fig. 2a) remained roughly constant during the first part of the event, with a slight increase before 14 UTC. At 19 UTC, when the surface front arrived at the measurement location, a rapid drop of about 2.5°C in 30 min was recorded. The temperature gradually declined further by about 3.5°C between 20 and 22 UTC and remained constant thereafter, resulting in an overall decrease in 2-m temperature of ~ 6°C. The local relative humidity (h; blue line in Fig. 2a) varies between $75-85\%$ before the frontal passage, and increases to values around $85-90\%$ thereafter.

The rain associated with this frontal event started in Zurich at 06 UTC 20 November and lasted until 03 UTC 21 November 2015. The total rain measured by a rain gauge on the rooftop was 30.9 mm, whereof 27.5 mm fell during the part of the event investigated here (07:00 - 23:30 UTC). The intensity varied between 0 and 3 mm h^{-1}, before increasing briefly to 10 mm h^{-1} as the surface front passed at 19 UTC (Fig. 2b). Thereafter, the intensity remained relatively high compared to the period prior to the frontal passage with an average of 3 mm h^{-1} until approximately 23 UTC, when it decreased to low values for the remainder of the event. Between 12 and 18 UTC, sustained wind speeds occurred between 5 and 10 m s^{-1}, and therefore the rain intensity was likely underestimated during this period due to the exposed location of the rain gauge. A nearby, less exposed meteorological station at ground level (MeteoSwiss Station Zurich Fluntern, at a distance of 1.3 km) recorded a total amount of rain of 38.3 mm during the event.

As an aside, we mention the decrease of the height of the 0°C isotherm due to the frontal passage. Two balloon soundings, launched from the measurement site in Zurich, indicate a decrease from 2700 m a.s.l. at 16:30 UTC to 1500 m a.s.l. at 22:30 UTC (not shown).

3.3 Isotopic composition of vapour and rain

The 10-minute averaged values were between -35‰ and -14‰ for $\delta^{18}O_v$ (not shown) and between -265‰ and -105‰ for δ^2H_v (Fig. 2c, black line). The vapour isotope measurements exhibit an overall decrease of more than 160‰ for δ^2H_v during the entire event. A weak decrease in δ^2H_v around 08 UTC was followed by a steady increase until 14 UTC. δ^2H_v slowly decreased thereafter until approximately 18 UTC when the decrease became steeper. It reached a minimum value at 23 UTC

Atmos. Chem. Phys. Discuss., https://doi.org/10.5194/acp-2018-482
Manuscript under review for journal Atmos. Chem. Phys.
Discussion started: 29 May 2018

Atmospheric Chemistry and Physics Discussions

and remained roughly constant thereafter. d_v rose from 5‰ to 20‰ during the event (Fig. 2d, black line). A gradual increase by about 5‰ before the arrival of the surface front was followed by a more rapid 10‰ increase in the 4 hours after the frontal passage. A distinct spike of 5‰ in d_v occurred just after the passage of the front at 19 UTC. Other short-term variations of d_v occurred within the uncertainty range.

Now we compare the equilibrium vapour from precipitation with the vapour isotope measurements to identify the possible influence of below-cloud processes. The isotopic signals of vapour (δ^2H_v; black line in Fig. 2c) and equilibrium vapour from the 86 rain samples ($\delta^2H_{p,eq}$; blue bars in Fig. 2c) exhibit a similar evolution during the whole event. Differences are overall less than 23‰. $\delta^2H_{p,eq}$ is more variable and its evolution is less smooth than for δ^2H_v. After an initial decrease with a subsequent increase similar to δ^2H_v, $\delta^2H_{p,eq}$ reaches two maxima at around 14 and 16 UTC, which coincide with low relative humidity and weak rain intensity. It decreases afterwards until the end of the sampling period. The decrease is particularly strong during the passage of the surface front and during the second distinct temperature drop (after 20:30 UTC). The overall evolution corresponds to a flat W-shape in the first part of the event until 16 UTC, and a strong decrease in the second part. This is similar to what Dütsch et al. (2016) found for a cold front in an idealised extratropical cyclone, but in our case without the increasing branch at the end, which may have occurred during the not sampled weak rain at the end of the event.

The $d_{p,eq}$ varies around 0‰ before 19 UTC, and then increases markedly during the passage of the front with values of more than 10‰. Notably, negative values of $d_{p,eq}$ occur during periods with weak rain (e.g., around 08:30, 13:30 and 16:00 UTC). d_v also increases during the event, but less abruptly and with less variations than $d_{p,eq}$. For further analysis, we split the event into two periods, a pre-frontal period until about 18:45 UTC (samples 1–54) and a post-frontal one (samples 55–86).

We now briefly consider correlations of the isotope time series with meteorological variables. $d_{p,eq}$ exhibits a positive correlation with h ($\rho = 0.88$) and rain intensity ($\rho = 0.63$). Smaller drops during phases with weak rain and low relative humidity experience enhanced evaporation, which decreases $d_{p,eq}$. The correlation with h is also strong for Δd ($\rho = 0.83$). The influence of rain evaporation also results in a negative correlation of $\Delta\delta$ with h ($\rho = -0.65$) and rain intensity ($\rho = -0.44$).

The similar evolution of δ^2H_v and $\delta^2H_{p,eq}$ in Fig. 2c indicates that equilibration of rain with the surrounding vapour plays an important role for the evolution of the time series. In order to facilitate the interpretation of measurements, a new framework is introduced below that makes the different physical processes more explicit.

4 A new interpretative framework for below-cloud processes

From comparing isotope signals in vapour and equilibrium vapour from precipitation, it appears that the difference between the two quantities would enable a more direct interpretation of different processes. Using the quantities $\Delta\delta$ and Δd (Eq. 6), the data is again displayed as time series (Fig. 3).

Some rain samples are in equilibrium with vapour for δ^2H (e.g., at 17 UTC), for d (at about 19 and 21 UTC) or for both (at 10 UTC). Other samples indicate the influence of evaporation with a positive $\Delta\delta$ and a strongly negative Δd (at about 14 and 16 UTC). Most post-frontal samples have a strongly negative $\Delta\delta$ and a Δd close to zero, which indicates the conservation of depleted $\delta^2H_{p,eq}$ from the cloud and incomplete equilibration with near-surface vapour. The identification and interpretation

Atmos. Chem. Phys. Discuss., https://doi.org/10.5194/acp-2018-482
Manuscript under review for journal Atmos. Chem. Phys.
Discussion started: 29 May 2018

Atmospheric Chemistry and Physics Discussions

of these processes from the new parameters $\Delta\delta$ and Δd is considerably more immediate than from the time-series of $\delta^2\mathrm{H_v}$, $\delta^2\mathrm{H_{p,eq}}$, d_v and $d_\mathrm{p,eq}$.

The influence of different processes becomes even more apparent when displaying the data using $\Delta\delta$ and Δd as coordinate axes in one diagram (Fig. 4). The origin of the diagram (0,0) indicates full equilibrium between vapour and precipitation. Rain samples of the 20 November 2015 event are displayed in the $\Delta\delta\Delta d$-space, sized by rain rate in Fig. 4a and coloured by sample number in Fig. 4b. Few data points are located in the vicinity of the origin, associated with intermediate rain rates during the pre-frontal phase of the event. Data points located to the left of the origin indicate that precipitation is more depleted than ambient air, and reflect a stronger cloud signal in precipitation. Most of the post-frontal data points with the most intense rain rates are located to the left of the origin. The data points seem to follow a line with a negative slope. A linear fit through the samples yields a regression line with a slope of $\frac{\Delta d}{\Delta\delta} = -0.31$ (Fig. 4a, solid black line). Rain falling through unsaturated air will lead to an increase in $\Delta\delta$ and a decrease in Δd.

It is noteworthy that similar slopes (-0.30 ± 0.02; dashed black lines in Fig. 4a) were found for three other cold fronts in Switzerland (Graf, 2018). This indicates that the slope may represent general characteristics of below-cloud evaporation and equilibration of rainfall during continental mid-latitude cold fronts.

Overall, the rain rate strongly influences the location of the samples in the diagram. Samples with the highest rain rates are located in the upper left corner, as they are less affected by below-cloud processes and retain more of their initial strongly negative $\Delta\delta$. Samples from periods with weak rain rates are located in the bottom right corner of the diagram, reflecting a stronger evaporation influence. In comparison, the influence of equilibration is weaker than of evaporation, which is indicated by the low number of points close to the origin of the diagram.

The regions in Fig. 4a that are covered by pre-frontal (purple) and post-frontal (green) samples are fairly well separated. This indicates that pre-frontal samples, which are on average higher in $\Delta\delta$ and lower in Δd, are more strongly affected by below-cloud processes than post-frontal samples. The difference can be explained by an on average lower rain intensity and a lower relative humidity during the pre-frontal phase, and therefore by enhanced below-cloud equilibration and evaporation. Additionally, the melting layer was clearly lower after the passage of the front, and thus both vertical distance and time for equilibration were reduced. Post-frontal samples therefore carry more of their depleted initial $\delta^2\mathrm{H_{p,eq}}$ from the cloud to the ground.

It is important to note that also other meteorological factors influence the isotopic evolution of sedimenting raindrops, in particular the detailed relative humidity profile, the formation height of precipitation, the isotope profile of vapour, and potential up- and downdrafts and turbulent motions below the cloud base. The effect of some of these processes can be investigated by considering measurements from different rainfall events, and, in particular, with the aid of idealised below-cloud interaction models. Such an analysis will be presented in a forthcoming paper.

From the analysis of the rainfall and vapour isotopes of the event on 20 November 2015, it appears that presenting data in the $\Delta\delta\Delta d$-space provides an insightful viewing device to decipher the complexity of below-cloud processes. In the next section, these findings are discussed in more general terms.

Atmos. Chem. Phys. Discuss., https://doi.org/10.5194/acp-2018-482
Manuscript under review for journal Atmos. Chem. Phys.
Discussion started: 29 May 2018

Atmospheric Chemistry and Physics Discussions

5 The influence of evaporation and equilibration

A $\Delta\delta\Delta d$-diagram shows the isotopic composition of equilibrium vapour from precipitation samples relative to the ambient surface vapour at the time when the samples were taken. The location of a precipitation sample in the $\Delta\delta\Delta d$-space is determined by two factors: (i) the initial composition of precipitation after formation in the cloud and (ii) the modification of this composition below the cloud by equilibration and evaporation. These below-cloud processes depend on the rain intensity: larger drops during intense rain are typically less affected by below-cloud processes because they spend less time in the air due to a faster fall velocity and they are more resilient to exchanges with the ambient vapour due to a smaller surface to volume ratio. The isotopic composition of a rain sample is a mass weighted average of the composition of all drops contained in a sample. The processes that act on a single drop are thus directly relevant for bulk precipitation.

The initial $\Delta\delta$ of a precipitating hydrometeor is strongly negative, because it is formed aloft from vapour that is depleted in δ^2H compared to vapour at the surface. The initial Δd of precipitation is uncertain, but assumed to be small. The increase of d_{v} with height (e.g., Bony et al., 2008; Sodemann et al., 2017) and non-equilibrium effects during precipitation formation in mixed-phase clouds, both increase $d_{\mathrm{p,eq}}$ (and Δd). This increase is however counteracted by a decrease of $d_{\mathrm{p,eq}}$ during the vapour-solid transition and by a decrease due to the non-linearity of the δ-scale (Dütsch et al., 2017).

Falling rain adopts the subsequently enriched δ^2H of the surrounding vapour through equilibration. If equilibration is efficient (light rain), the isotopic difference to the surrounding vapour becomes small and rain exhibits small absolute values of $\Delta\delta$ and Δd when it arrives at the ground. Strongly equilibrated samples are thus located close to the origin (0,0) in Fig. 4. If equilibration is not efficient (intense rain), rain retains more of its initial low δ^2H and arrives at the ground with a negative $\Delta\delta$. Weakly equilibrated samples are thus typically located in the upper left of Fig. 4.

The preferential loss of light isotopes and non-equilibrium effects during evaporation of rain will increase $\delta^2\mathrm{H}_{\mathrm{p,eq}}$ (and $\Delta\delta$) and decrease $d_{\mathrm{p,eq}}$ (and Δd). Rain samples that are strongly affected by evaporation will thus be located in the bottom right quadrant of the $\Delta\delta\Delta d$-diagram. The location of a sample in the $\Delta\delta\Delta d$-space therefore contains information about the intensity and type of below-cloud processes, because they act differently on the isotopic composition of rain.

6 Conclusions

The processes acting on precipitation as it falls from the cloud base to the surface are complex and difficult to access. Using highly resolved measurements of stable isotopes in vapour and rain at the surface, we identify an integrated signal of these so-called below-cloud processes using a new interpretation framework. The $\Delta\delta\Delta d$-diagram is proposed as a valuable means of displaying measurement data (or model data) of both δ^2H and d simultaneously. It shows the isotopic composition of equilibrium vapour from precipitation relative to near-surface vapour. $\Delta\delta$ is shown along the x-axis and Δd along the y-axis, which combines $\delta^2\mathrm{H}_{\mathrm{v}}$, $\delta^2\mathrm{H}_{\mathrm{p,eq}}$, d_{v} and $d_{\mathrm{p,eq}}$ in a single diagram. To display data in the $\Delta\delta\Delta d$-space, the isotopic composition of surface vapour and precipitation have to be known, as well as surface temperature to calculate $\delta^2\mathrm{H}_{\mathrm{p,eq}}$ and $d_{\mathrm{p,eq}}$. The usefulness of this diagram has been illustrated with measurements from a cold frontal rain event in Switzerland. The main conclusions from this study are:

1. Equilibration between vapour and rain and evaporation of rain in unsaturated air leave distinct imprints in the isotope signal of surface rain. Both aspects of the molecular exchange between the liquid and solid phase become more accessible by quantifying the deviation from isotopic equilibrium with the surface vapour with the two quantities $\Delta\delta$ and Δd.

2. The $\Delta\delta\Delta d$-diagram facilitates the interpretation of the effect of below-cloud processes on rain samples by jointly displaying the degree of equilibration between rain and vapour and the influence of evaporation using the newly defined variables $\Delta\delta$ and Δd. Equilibration and evaporation have different pathways in the $\Delta\delta\Delta d$-space, where they are more distinguishable than in a time series. Investigating rain samples in the $\Delta\delta\Delta d$-space is therefore complementary to a time series perspective, in particular when data points are further coloured or sized using additional parameters, such as rainfall rate.

3. Samples from the 20 November 2015 cold front show that evaporation is the dominant process, while equilibration without evaporation appears as an exception. Evaporation is strongly related to rain rate, which was less intense during the pre-frontal period.

4. Post-frontal samples are less equilibrated and evaporated than pre-frontal samples, due to higher below-cloud relative humidity and a lower temperature and melting layer after the frontal passage.

5. Evaporation causes data points in the $\Delta\delta\Delta d$-space to follow a line with a negative slope of $\frac{\Delta d}{\Delta\delta} = -0.31$. Similar slopes were obtained for several other frontal rain events, suggesting that the characteristics of below-cloud processes, as revealed by the $\Delta\delta\Delta d$-diagram are similar for this kind of rain events.

Using the $\Delta\delta\Delta d$ framework, it will be highly valuable to investigate the below-cloud effects for other precipitation events. For example, a snowfall event, or a transition from rain to snow could show a stronger cloud signal due to the absent exchange between vapour and solid. Cases of drizzle could exhibit a large degree of equilibration between small drops and ambient vapour. Cases of convective rainfall could show variations between more cloud-related signals in downdrafts and stronger evaporation and equilibration in updrafts.

We expect that the analysis of the isotopic composition during rain events at other locations and model studies will benefit from using the parameters $\Delta\delta$ and Δd, and the $\Delta\delta\Delta d$-diagram as additional viewing device to obtain insight into below-cloud processes. Thereby, further constraints on microphysical processes in models can be obtained, and ultimately contribute to a more complete use of stable water isotopes to build internally consistent water cycles into numerical weather prediction and climate models.

Atmos. Chem. Phys. Discuss., https://doi.org/10.5194/acp-2018-482
Manuscript under review for journal Atmos. Chem. Phys.
Discussion started: 29 May 2018

Atmospheric Chemistry and Physics Discussions

Table 1. Calculated equilibrium difference (Δ_{l-v}) of vapour in equilibrium with liquids of different isotopic composition (A and B). The fractionation factors of Majoube (1971) are used for the calculations.

composition of liquid		Δ_{l-v} @ 20°C	Δ_{l-v} @ 0°C	
	0‰	78.4‰	101.0‰	δ^2H
A	0‰	9.7‰	11.6‰	δ^{18}O
	0‰	0.8‰	8.3‰	*d*
	−120‰	69.0‰	88.9‰	δ^2H
B	−15‰	9.6‰	11.4‰	δ^{18}O
	0‰	−7.5‰	−2.4‰	*d*

Atmos. Chem. Phys. Discuss., https://doi.org/10.5194/acp-2018-482
Manuscript under review for journal Atmos. Chem. Phys.
Discussion started: 29 May 2018

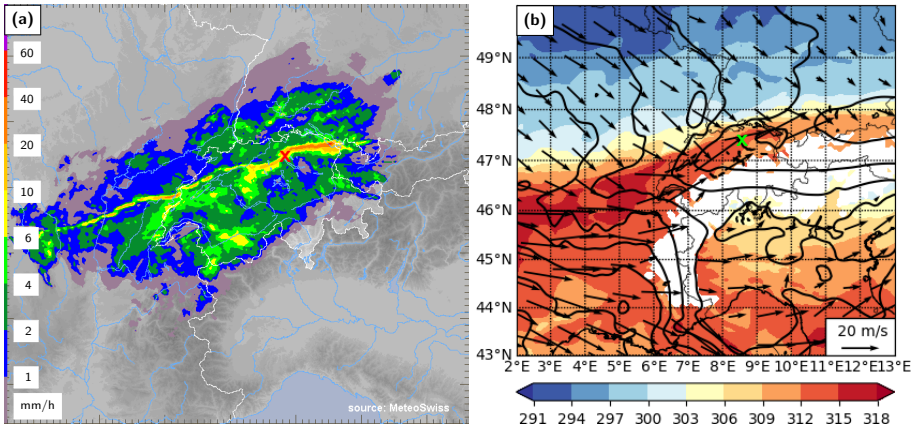

Figure 1. (a) Radar composite of surface rain intensity from MeteoSwiss at 19 UTC 20 November 2015, when the surface front passed over the measurement site. (b) Equivalent potential temperature (Θ_e in K, colour) and horizontal wind (arrows) at 850 hPa from COSMO-2 analysis data at 19 UTC 20 November 2015. The location of the measurement site Zurich is indicated by a red and a green cross, respectively.

Atmos. Chem. Phys. Discuss., https://doi.org/10.5194/acp-2018-482
Manuscript under review for journal Atmos. Chem. Phys.
Discussion started: 29 May 2018

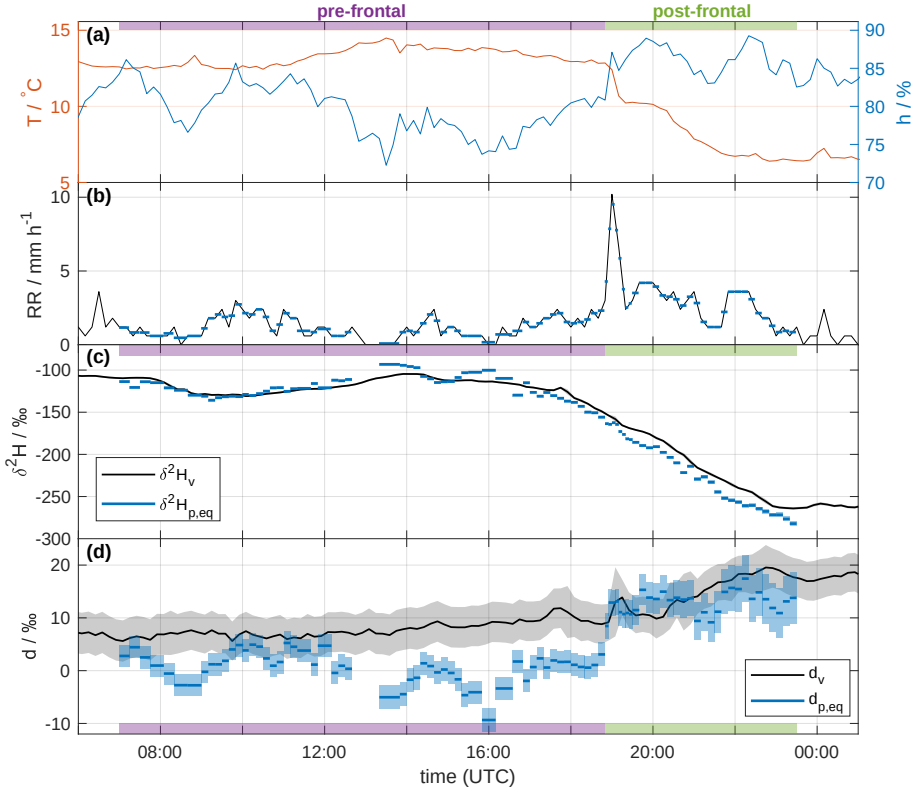

Figure 2. Time series of observations in Zurich between 06 UTC 20 November and 01 UTC 21 November 2015. (a) Local temperature (T; red) and relative humidity (h; blue) measured by the meteorological station. (b) Rain intensity from the rain gauge (black). Blue bars indicate the average values for each rain sample period. (c) δ^2H of near-surface vapour (10 min averaged δ^2H_v; black line) and of the equilibrium vapour from precipitation ($\delta^2H_{p,eq}$; blue bars). The width of the blue bars denotes the period over which the rain samples were collected. (d) Same as in (c), but for d. The calibrated uncertainties are indicated by the shaded areas (hardly or not visible for δ^2H_v and $\delta^2H_{p,eq}$). Pre- and post-frontal periods are indicated with purple and green bars, respectively.

Atmos. Chem. Phys. Discuss., https://doi.org/10.5194/acp-2018-482
Manuscript under review for journal Atmos. Chem. Phys.
Discussion started: 29 May 2018

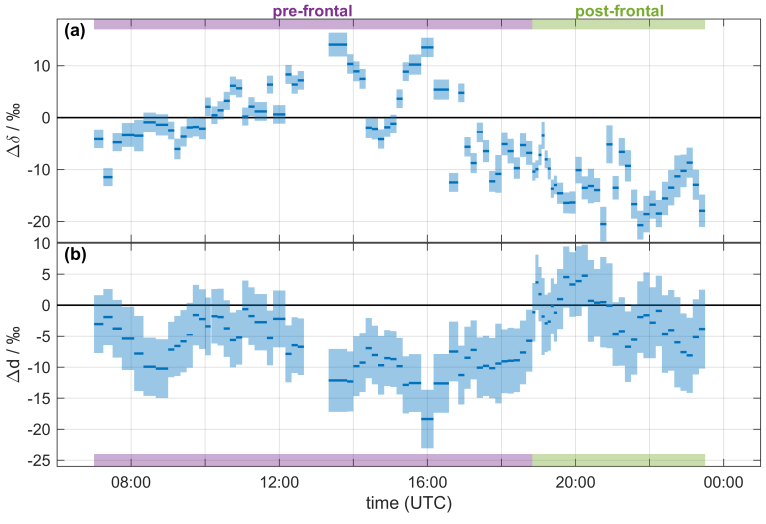

Figure 3. Time series of (a) $\Delta\delta$ and (b) Δd of the precipitation samples collected on 20 November 2015. The width of the blue bars denotes the period over which the rain samples were collected. The calibrated uncertainties are indicated by the shaded areas. Pre- and post-frontal periods are indicated with purple and green bars, respectively.

Atmos. Chem. Phys. Discuss., https://doi.org/10.5194/acp-2018-482
Manuscript under review for journal Atmos. Chem. Phys.
Discussion started: 29 May 2018

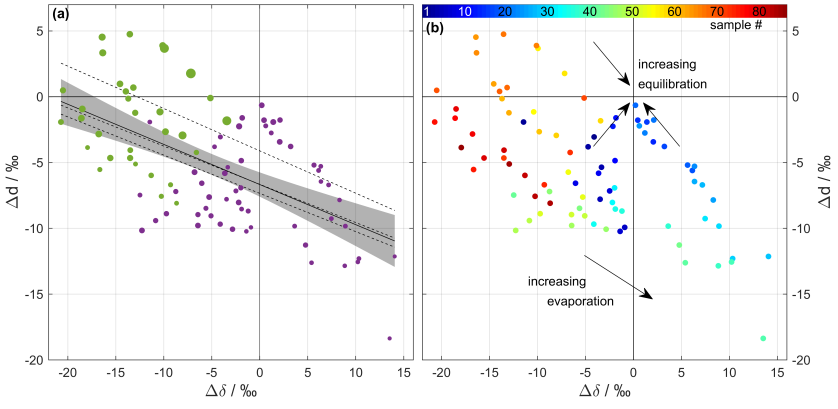

Figure 4. $\Delta\delta\Delta d$-diagram for the precipitation samples collected on 20 November 2015. (a) Pre-frontal samples are coloured in purple and post-frontal ones in green. The size of the circle corresponds to the average rain intensity of the sample. The solid black line represents a linear fit through all samples with the 95% confidence band in shading. Dashed black lines correspond to the linear fits through the samples of 3 other events (cf. text). (b) Same samples as in (a), but coloured according to their number (see legend) to highlight the evolution $\Delta\delta$ and Δd in time.

Competing interests. The authors declare that they have no conflict of interest.

Data availability. All observation data presented in this study are available from the authors upon request (pascal.graf@env.ethz.ch).

Acknowledgements. We thank Patrick Bertollini for his help with precipitation sampling and analysis, Peter Isler for the meteorological data, Barbara Herbstritt (University of Freiburg) and Yongbiao Weng (University of Bergen) for reference measurements of our calibration standards, and Stephan Pfahl, Franziska Aemisegger and Marina Dütsch for discussions and inputs. HS acknowledges funding from the Norwegian Research Council projects SNOWPACE (Project No. 262710) and FARLAB (Project No. 245907).

References

Aemisegger, F.: Atmospheric stable water isotope measurements at the timescale of extratropical weather systems, Ph.D. Thesis, Diss. ETH No. 21165, ETH Zurich, https://e-collection.library.ethz.ch/view/eth:7474, 2013.

Aemisegger, F., Sturm, P., Graf, P., Sodemann, H., Pfahl, S., Knohl, A., and Wernli, H.: Measuring variations of δ18O and δ2H in atmospheric water vapour using two commercial laser-based spectrometers: an instrument characterisation study, Atmos. Meas. Tech., 5, 1491–1511, https://doi.org/10.5194/amt-5-1491-2012, 2012.

Aemisegger, F., Spiegel, J. K., Pfahl, S., Sodemann, H., Eugster, W., and Wernli, H.: Isotope meteorology of cold front passages: A case study combining observations and modeling, Geophys. Res. Lett., 42, 5652–5660, https://doi.org/10.1002/2015GL063988, 2015.

Barras, V. and Simmonds, I.: Observation and modeling of stable water isotopes as diagnostics of rainfall dynamics over southeastern Australia, J. Geophys. Res. Atmos., 114, D23 308, https://doi.org/10.1029/2009JD012132, 2009.

Bennett, L. J., Browning, K. A., Blyth, A. M., Parker, D. J., and Clark, P. A.: A review of the initiation of precipitating convection in the United Kingdom, Q. J. R. Meteorol. Soc., 132, 1001–1020, https://doi.org/10.1256/qj.05.54, 2007.

Bony, S., Risi, C., and Vimeux, F.: Influence of convective processes on the isotopic composition (δ18O and δD) of precipitation and water vapor in the tropics: 1. Radiative-convective equilibrium and Tropical Ocean–Global Atmosphere–Coupled Ocean-Atmosphere Response Experiment (TOGA-COARE) simulations, J. Geophys. Res. Atmos., 113, D19 305, https://doi.org/10.1029/2008JD009942, 2008.

Celle-Jeanton, H., Gonfiantini, R., Travi, Y., and Sol, B.: Oxygen-18 variations of rainwater during precipitation: application of the Rayleigh model to selected rainfalls in Southern France, J. Hydrol., 289, 165–177, https://doi.org/10.1016/j.jhydrol.2003.11.017, 2004.

Cooney, J.: Remote measurements of atmospheric water vapor profiles using the Raman component of laser backscatter, J. Appl. Meteor., 9, 182–184, 1970.

Coplen, T. B., Neiman, P. J., White, A. B., Landwehr, J. M., Ralph, F. M., and Dettinger, M. D.: Extreme changes in stable hydrogen isotopes and precipitation characteristics in a landfalling Pacific storm, Geophys. Res. Lett., 35, L21 808, https://doi.org/10.1029/2008GL035481, 2008.

Dansgaard, W.: Stable isotopes in precipitation, Tellus, 16, 436–468, 1964.

Dütsch, M., Pfahl, S., and Wernli, H.: Drivers of δ2H variations in an idealized extratropical cyclone, Geophys. Res. Lett., 43, 5401–5408, https://doi.org/10.1002/2016GL068600, 2016.

Dütsch, M., Pfahl, S., and Sodemann, H.: The impact of nonequilibrium and equilibrium fractionation on two different deuterium excess definitions, J. Geophys. Res. Atmos., 122, 12,732–12,746, https://doi.org/10.1002/2017JD027085, 2017.

Galewsky, J., Steen-Larsen, H. C., Field, R. D., Worden, J., Risi, C., and Schneider, M.: Stable isotopes in atmospheric water vapor and applications to the hydrologic cycle, Rev. Geophys., 54, 409–465, https://doi.org/10.1002/2015RG000512, 2016.

Graf, P.: The effect of below-cloud processes on short-term variations of stable water isotopes in surface precipitation, Ph.D. Thesis, Diss. ETH No. 24777, ETH Zurich, 2018.

IAEA: Reference sheet for international measurement standards VSMOW2 and SLAP2, Int. At. Energy Agency IAEA Vienna, 2009.

Lee, J.-E. and Fung, I.: "Amount effect" of water isotopes and quantitative analysis of post-condensation processes, Hydrol. Process., 22, 1–8, https://doi.org/10.1002/hyp.6637, 2008.

Majoube, M.: Fractionnement en oxygène 18 et deutérium entre l'eau et sa vapeur, J. Chim. Phys., 68, 1423–1436, 1971.

Managave, S. R., Jani, R. A., Rao, T. N., Sunilkumar, K., Satheeshkumar, S., and Ramesh, R.: Intra-event isotope and raindrop size data of tropical rain reveal effects concealed by event averaged data, Clim. Dyn., 47, 981–987, https://doi.org/10.1007/s00382-015-2884-7, 2016.

Miyake, Y., Matsubaya, O., and Nishihara, C.: An isotopic study on meteoric precipitation, Pap. Meteorol. Geophys., 19, 243–266, 1968.

Muller, C. L., Baker, A., Fairchild, I. J., Kidd, C., and Boomer, I.: Intra-event trends in stable isotopes: Exploring midlatitude precipitation using a vertically pointing micro rain radar, J. Hydrometeor., 16, 194–213, https://doi.org/10.1175/JHM-D-14-0038.1, 2015.

Risi, C., Bony, S., Vimeux, F., Chong, M., and Descroix, L.: Evolution of the stable water isotopic composition of the rain sampled along Sahelian squall lines, Q. J. R. Meteorol. Soc., 136, 227–242, https://doi.org/10.1002/qj.485, 2010.

Roberts, A. and Knippertz, P.: Haboobs: convectively generated dust storms in West Africa, Weather, 67, 311–316, https://doi.org/10.1002/wea.1968, 2012.

Schneider, M. and Hase, F.: Ground-based FTIR water vapour profile analyses, Atmos. Meas. Tech., 2, 609–619, https://doi.org/10.5194/amt-2-609-2009, 2009.

Seity, Y., Brousseau, P., Malardel, S., Hello, G., Bénard, P., Bouttier, F., Lac, C., and Masson, V.: The AROME-France convective-scale operational model, Mon. Wea. Rev., 139, 976–991, https://doi.org/10.1175/2010MWR3425.1, 2010.

Skamarock, C., Klemp, B., Dudhia, J., Gill, O., Barker, D., Duda, G., Huang, X.-Y., Wang, W., and Powers, G.: A description of the advanced research WRF version 3, NCAR Tech. Note NCARTN-475STR, https://doi.org/10.5065/D68S4MVH, 2008.

Sodemann, H., Aemisegger, F., Pfahl, S., Bitter, M., Corsmeier, U., Feuerle, T., Graf, P., Hankers, R., Hsiao, G., Schulz, H., Wieser, A., and Wernli, H.: The stable isotopic composition of water vapour above Corsica during the HyMeX SOP1 campaign: Insight into vertical mixing processes from lower-tropospheric survey flights, Atmos. Chem. Phys., 17, 6125–6151, https://doi.org/10.5194/acp-17-6125-2017, 2017.

Solheim, F., Godwin, J. R., Westwater, E. R., Han, Y., Keihm, S. J., Marsh, K., and Ware, R.: Radiometric profiling of temperature, water vapor and cloud liquid water using various inversion methods, Radio Sci., 33, 393–404, https://doi.org/10.1029/97RS03656, 1998.

Steppeler, J., Doms, G., Schättler, U., Bitzer, H. W., Gassmann, A., Damrath, U., and Gregoric, G.: Meso-gamma scale forecasts using the nonhydrostatic model LM, Meteorol. Atmos. Phys., 82, 75–96, https://doi.org/10.1007/s00703-001-0592-9, 2003.

Stewart, M. K.: Stable isotope fractionation due to evaporation and isotopic exchange of falling waterdrops: Applications to atmospheric processes and evaporation of lakes, J. Geophys. Res., 80, 1133–1146, https://doi.org/10.1029/JC080i009p01133, 1975.

Wang, S., Zhang, M., Che, Y., Zhu, X., and Liu, X.: Influence of below-cloud evaporation on deuterium excess in precipitation of arid Central Asia and its meteorological controls, J. Hydrometeor., 17, 1973–1984, https://doi.org/10.1175/JHM-D-15-0203.1, 2016.

Xie, X., Evaristo, R., Troemel, S., Saavedra, P., Simmer, C., and Ryzhkov, A.: Radar observation of evaporation and implications for quantitative precipitation and cooling rate estimation, J. Atmos. Oceanic Technol., 33, 1779–1792, https://doi.org/10.1175/JTECH-D-15-0244.1, 2016.

Yoshimura, K., Kanamitsu, M., and Dettinger, M.: Regional downscaling for stable water isotopes: A case study of an atmospheric river event, J. Geophys. Res. Atmos., 115, D18 114, https://doi.org/10.1029/2010JD014032, 2010.